A toy model to understand the inertial layer dynamics in turbulent boundary layers

J.C. Cuevas Bautista*
University of New Hampshire, Department of Mechanical Engineering, Durham 03824, USA.
(Dated: July 13, 2016)

Recent studies indicate that the inertial layer structure of the turbulent boundary layer at high Reynolds number (Re) is composed of large uniform momentum zones segregated by narrow fissures of concentrated vorticity. Experiments reveal that the dimensionless fissures thickness (scaled by boundary layer thickness) is $\mathcal{O}(1/\sqrt{Re})$ and the dimensionless streamwise velocity jump across a fissure scales with the friction velocity $\mathcal{O}(u_\tau)$. A toy model that captures the essential elements of the turbulent boundary layer structure at high Re is constructed to evaluate the long-time averaged flow statistics of the boundary layer. First, a "master" instantaneous streamwise velocity profile in the wall-normal direction is constructed by placing a discrete number of fissures across the boundary layer thickness. The number of fissures and their wall-normal locations follow scalings informed by analysis of mean momentum equation. The wall-normal positions of the fissures are allowed then to randomly move in the wall-normal direction creating a statistically independent instantaneous velocity profile. This process is then repeated to create an ensemble of instantaneous velocity profiles from which average statistics of the turbulent boundary layer are computed and assessed. The statistics of the toy model are compared to statistics acquired in turbulent boundary layers at high Re.

I. INTRODUCTION

Turbulent boundary layers and their mechanism are one the most active research areas in fluid mechanics [1–3]. Due to their chaotic behaviour, models that make statistical predictions are attractive. In this regard, there is general consensus in the scientific community that turbulent boundary layers exhibit similar statistical properties, hence most studies rely on the reproducibility of averaging techniques. As a consequence, part of the flow history is lost in this approach. Herein we attempt to explain the mean streamwise velocities as the product of the long-time average of multiple instantaneous velocity profiles with different spatial arrangements of uniform momentum zones (UMZs). This work builds upon the initial observations of Adrian and co-workers as now described.

We focus on two important observations that Adrian *et al.* [4] made about the structure of turbulent boundary layers. One is that zones of remarkably constant streamwise momentum exist throughout the outer part of the boundary layer. A second is that these regions seem to be bounded by thin regions of elevated vorticity. From here relatively low Reynolds number study Adrian *et al.* [5] surmised that these vortical fissures are the concatenation of a cluster of hairpin vortex heads associated with a packet of hairpin vortices. At much higher Reynolds numbers Priyadarshana *et al.* [6] and Morris *et al.* [7] found that the fissure structure was more like a turbulent shear layer. They also indicated that these structural properties are exclusive of the instantaneous velocity profiles which contribute to the mean statistical properties. More recently de Silva *et al.* [8] studied the presence of UMZs in turbulent boundary layers by comparing particle image velocimetry (PIV) data sets with synthetic instantaneous velocity fields. The established criteria to detect UMZs involves computing the probability density function (p.d.f.) of random instantaneous PIV velocity profiles. The UMZs are associated with the local maxima (modal velocity) in this p.d.f., and the number of UMZs are determined by the modal velocities. The same analysis was applied to the synthetic velocity fields which also evidenced different modal velocities in the instantaneous p.d.fs. We remark unlike of [8] in our toy model the existence of UMZs is already assumed and it pretends to explain how they are distributed and affect the mean streamwise statistics in the turbulent boundary layer.

In contrast with the traditional statistical approach, constructing the mean velocity profile by superposition of instantaneous velocity profiles with a different UMZs distribution allow us to examine in detail the individual history of the flow and explain the layers structure of turbulent flows. The phenomenological and experimental description of the structure and origin of the uniform momentum zones through boundary layer has been studied by several authors [4, 5, 8]. They suggest that UMZ are the result of the interaction of a wider range of structures that populate the turbulent boundary layer[5] such as hairpins and streamwise vortices. Adrian *et al.* [5] have made a thoroughly study about how the vortex structures are organized and segregate the UMZs in turbulent boundary layers. An important conceptual scenario noted by [5] states that packets of vortex structures aligns in the streamwise direction creating a net effect of zones with a quasi-uniform momentum. Vortex structures are also referred as vortical fissures or vortex tubes when they represent the transversal section of a hairpin vortex in the streamwise-wall normal plane [5]. Priyadarshana *et al.* [6] makes a good representation of the vortical fissures and their distribution in the instantaneous streamwise

* jcc1@wildcats.unh.edu

velocity profile (see Fig. 1). Vortical fissures are zones of concentrated vorticity that can be spread by turbulent advection to regions where the mean viscous force is negligible. It has been shown using dimensional analysis and scaling arguments that the thickness of the vortical fissures scales with the Reynolds as $\mathcal{O}(1/\sqrt{Re})$ [9], thus as Re increases, the thickness of the vortical fissures decreases. In the toy model presented here the thickness of vortical fissures is assumed negligible.

The zonal arrangement represented in Fig. 1 could give us an insight to the traditional structure of layers in the mean velocity profile. In the proposed model here, this is explored by using different statistical distribution for perturbing the wall normal position of the vortical fissures (see Sec. II). Some models have achieved notable results in reproduce the dynamics and the statistical properties of turbulent boundary layers by using different structures as hairpin structures [10] or eddy structures [11]. However these models depend directly in the attached eddy hypothesis where the geometry of the eddies arising from the wall must be known in order to reproduce correctly the wall and the wake structure of the boundary layer. The model employed herein does not depend on specific geometries, instead it is based in the existence of two structure motions, UMZs and vortical fissures. These later are allowed to move randomly through the boundary layer following a scaling for the inertial region derived from MMB theory (see Sec II B). The analysis of this scaling would help to explain the boundaries and the physical properties of the mean structure of the turbulent boundary layers (see Sec II A). In this paper we present a simplified toy model to reproduce the higher order moments of the streamwise turbulent boundary layers. The numerical model can be tweaked in such way that we can verify if the long-time average of the instantaneous uniform-momentum zonal structures reproduces reasonably the physical and statistical properties of turbulent wall-bounded flows. Regarding this, different boundary conditions are explored in the layers I, II and III of the four-layer structure (see Sec II A). DNS data for a channel flow at friction Reynolds number $\delta^+ = \delta u_\tau/\nu \approx 5200$ [12] (where $u_\tau = \sqrt{\tau_\omega/\rho}$ is the friction velocity, τ_ω is the mean wall shear stress, ν is the kinematic viscosity and δ is the boundary layer thickness) along with scaling reported by MMB theory was used to build the model.

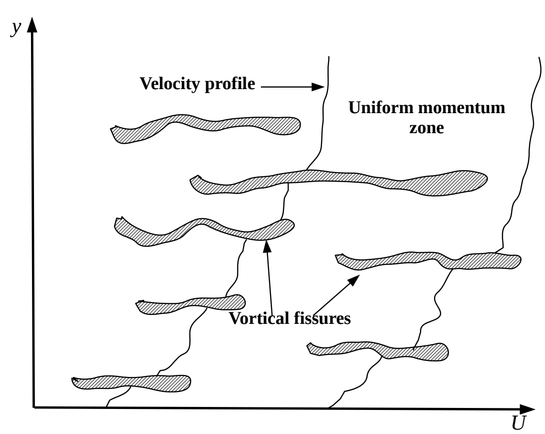

FIG. 1. Pictorial representation of instantaneous velocity profiles like zones of uniform momentum separated by zones of concentrated vorticity (vortical fissures). Where U is the mean velocity in the x direction (streamwise) and y is the wall normal coordinate. Adapted from [6]

II. NUMERICAL METHODS

A. Four-layer structure

The traditional hierarchy of layers in turbulent boundary layers, i.e. the viscous sublayer, buffer layer, logarithmic layer and the outer layer is described extensively in standard textbooks on turbulence [13–15]. However we will provide a briefly discussion about the layers structure based in the alternative approach of the MMB theory [16, 17]. Klewicki *et al.* [18] also describes in detail how the MMB theory predicts the physical and scaling behaviours of the so called four-layer structure in wall bounded-flows in analogy with the classical theory. The velocity and length scales of the emergent four-layer structure in the mean streamwise velocity profile are summarized in Table I.

TABLE I. Scaling associated to the four layer structure from MMB theory. Δy represents the thickness of the layer while Δu is the velocity increment associated to that layer in the turbulent boundary layer [18].

Layer	Δy	Δu
I	$\mathcal{O}(\nu/u_\tau)(\lesssim 3)$	$\mathcal{O}(u_\tau)(\lesssim 3)$
II	$\mathcal{O}(\sqrt{\nu\delta/u_\tau})(\simeq 1.6)$	$\mathcal{O}(U_\infty)(\simeq 0.5)$
III	$\mathcal{O}(\sqrt{\nu\delta/u_\tau})(\simeq 1.0)$	$\mathcal{O}(u_\tau)(\simeq 1)$
IV	$\mathcal{O}(\delta)(\to 1)$	$\mathcal{O}(U_\infty)(\to 0.5)$

The length and velocity increments have been normalized by the viscous scales ν and u_τ and the outer units δ and the free-stream velocity U_∞. The four-layer structure is the result of the dynamical balance of the terms in the mean momentum equation (MME) for a boundary layer flow (a similar structure remains for a channel flow [18])

$$U^+\frac{\partial U^+}{\partial x^+} + V^+\frac{\partial U^+}{\partial y^+} = \frac{\partial^2 U^+}{\partial y^{+2}} + \frac{\partial T^+}{\partial y^+}. \qquad (1)$$

Where the superscript '+' denotes normalization by the viscous scales and the capital letters are mean quantities. $T^+ = -\langle uv\rangle^+$ is the Reynold stress. The left hand-side term in Eq. 1 represents the inertial force while the right hand-side terms represent the viscous and Reynolds stress gradients. Layer I is the equivalent to the viscous sublayer in the conventional theory, here the viscous forces predominates over the turbulent inertia force. Layer II is denominated the stress gradient balance layer, since the gradients of the Reynolds and viscous stresses are approximately equal. Layer III is the mesolayer, here all the forces in Eq. 1 are approximately of the same order of magnitude. In this layer the Reynolds stress presents its maximum value, this is attributed to the transition from attached to detached eddies (Ref.[18], p. 833). Lastly, layer IV correspond to the classical wake layer. In the toy model proposed here we attempt to reproduce and describe the structure of layer II and III which mostly conform the traditional logarithmic layer.

B. Model

A mean step master stream-wise velocity profile is represented within the boundary layer by a set of N discrete velocity steps spaced according to

$$U^+_{i+1} = U^+_i + \phi_c^2 ln(\phi_c), \tag{2}$$
$$y^+_{i+1} = \phi_c y^+_i \quad i = 0, \dots, N-1. \tag{3}$$

As noted by Klewicki *et al.* [19], expressions (2) and (3) estimate approximately the mean velocity and the width of the layers in the inertial domain (See table I for comparison). In our step model, (2) determines the increments in the stream-wise normalized velocity U^+, the width of the steps in the x coordinate while (3) determines the increments in the normalized wall normal position y^+, the height of the steps in the y coordinate (See Fig. 2). The golden ratio ϕ_c is given by $\phi_c = (1+\sqrt{5})/2$ [19] and the thickness of the vortical fissures $\mathcal{O}(1/\sqrt{Re})$ is considered negligible at high Re. For the lower boundary condition, we have assumed that $y^+_0 = \phi_c\sqrt{\delta^+}$ in order to coincide with the onset of the logarithmic region, while $U^+_0 = 0.5U^+_\infty$ to be the half of the normalized free-stream velocity U^+_∞ (see scaling for layer II in table I). In addition, the velocity for the first UMZ from $y^+ = 0$ to $y^+ = y^+_0$ is held fixed at $U^+_0 = 0.5U^+_\infty$. The upper boundary condition ensure that the last position y^+_N of the vortical fissure and its associated velocity U^+_N be constrained by $y^+_N \approx \delta^+$.

Fig. 2 illustrates the mean step master velocity profile with a grid of 5481 linearly spaced positions in the wall normal direction, each one with an associated streamwise velocity. The black dots are the velocities and positions of the vortical fissures computed using (2) and (3) respectively. Then the zones of uniform momentum are created by allocating the velocity of the current vortical fissure to the grid points between the previous y_{i-1} and the current vortical fissure y_i. This velocity remains characteristic for each vortical fissure, thus we wave $N-1$ uniform momentum zones, where N is number of the vortical fissures. Note that at higher δ^+ the number of UMZs increases. Next, instantaneous velocity profiles are created by the

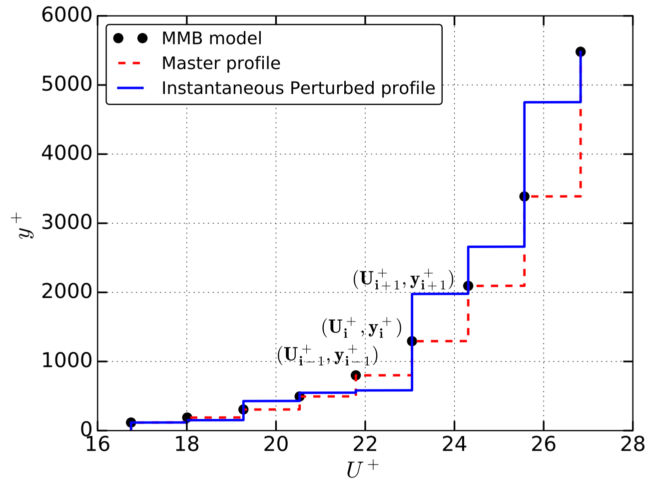

FIG. 2. Mean step velocity master profile (red dashed lines) overlapped with an instantaneous perturbed velocity profile (blue solid line) and the original data points (filled black circles) computed by Eqs. (2) and (3). $\delta^+ = 5200$ and $U^+_\infty = 26.5$ are from channel DNS [12].

repositioning of the vortical structures through the wall normal direction. This is accomplished by add a perturbation of the actual height $\Delta h^+_i = y^+_i - y^+_{i-1}$ of the UMZ to the current position of the vortical fissure y^+_i, i.e,

$$y^+_{new} = y^+_i \pm \Delta h^+_i * PERT. \tag{4}$$

PERT stands for any statistical distribution used into perturb the height of the UMZ (e.g. Gaussian, uniform exponential, beta, etc). Here we remark that just the position of the vortical fissures are being perturbed though the velocities remains attached to each vortical fissure. Thus zones of higher momentum can reside closer to the wall if the upper vortical fissures move enough downward in the boundary layer. Once the new positions have been computed, we proceed to fill the grid points similarly to the master profile. Fig. 2 shows how most of the verticals fissure have moved upward excepting the second and fifth that have moved downward respect to their original positions (blue solid line). Fig. 3 shows five instantaneous velocity step profiles, it can be seen how the upper vortical fissures resides now in the vicinity of the wall and some lower vortical fissures have moved to intermediate positions, this mechanism allow us to create zones of negative vorticity since the uniform momentum zones are not increasing monotonically.

The multiple instantaneous step velocity profiles are considered independent events since they are the result of the statistical perturbation in the wall normal positions of the master profile.

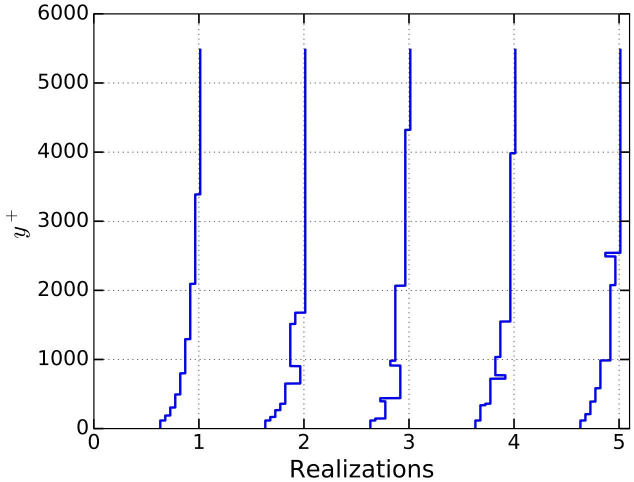

FIG. 3. Multiple instantaneous velocity profiles with a gaussian perturbation of mean $\mu = 0$ and standard deviation $\sigma = 0.4$.

III. MEAN TURBULENCE STATISTICS ANALYSIS

For the purpose of validate the toy model, the high order moments such as the mean, variance, skewness and kurtosis of the mean turbulent streamwise velocity profile were computed. As described in Sec. II, different statistical distributions were used to randomize the positions of the vortical fissures, however excepting for the uniform and Gaussian distribution, all of them always showed a poor agreement as qualitative as quantitatively compared with the experimental results (See [20] for experimental streamwise higher order moments). Regarding this, we present here the results for the Gaussian and uniform distribution respectively. Other consideration pertaining to the statistical convergence is the number of independent realizations in the average process. It was considered a big range of realizations between 10 up to 20000. It was found that after 5000 realizations the qualitative shape of the higher order moments does not show significant changes. Therefore 5000 independent realizations are selected like criteria of good convergence for the averaging.

A. Gaussian perturbation

Multiple scenarios with different standard deviations σ for the Gaussian perturbation were investigated, the two more representative are presented here. They represent poor ($\sigma = 0.4$) and good ($\sigma = 1$) agreement with the experimental results [20, 21], both with a mean of $\mu = 0$. First scenario considers that the random variation in the position of the vortical fissures ranges between -120% and 120% of their current positions, where 3σ events are less likely to occur. Fig. 4 shows the turbulent mean velocity profile for $\sigma = 0.4$, it can be appreciated regions of relative uniform velocity along with small velocity jumps located close to the unperturbed wall normal positions of the vortical fissures (see Fig. 2). These oscillations are similar to the peak-locking phenomena in experimental data, and they are the result of the velocity average of vortical fissures with identical velocities in the same wall normal positions (See Appendix A for a mathematical model that explains the oscillations in the streamwise statistics). Also note that an uniform momentum zone arise from $y^+ = 0$ to $y^+ = 118$, these are the velocity boundary conditions imposed in the first position of the vortical fissure which are held fixed. Despite of these discrepancies, the mean velocity profile shows an acceptable agreement with the shape of the experimental data.

Fig. 5 shows the variance of the streamwise fluctuations for 5000 independent realizations as a function of the wall normal position. Here the peak-locking phenomena is more evident and it is explained by use the Eq. A1 and considering the special rules in the toy model explained in Appendix A. Since most of the random number for a Gaussian distributions are distributed around the mean, in this case $\mu = 0$. Then the probability to have a vortical fissure in the same position as the master profile is bigger than any other position (Eq. 4). Consequently the number of vortical fissures with the same velocity will be distributed symmetrically around the original position in the master profile (red vertical dashed lines). It is also remarkable that for this scenario crossing vortical fissures are rarely observed since the random perturbation does not exceed 130% units of their current wall normal positions.

The skewness for the streamwise fluctuations (Fig. 6) is plotted on a semi-logarithmic axes plot as a function of the wall normal position. The graph shows the correct trend in the lower and the upper edge of the inertial

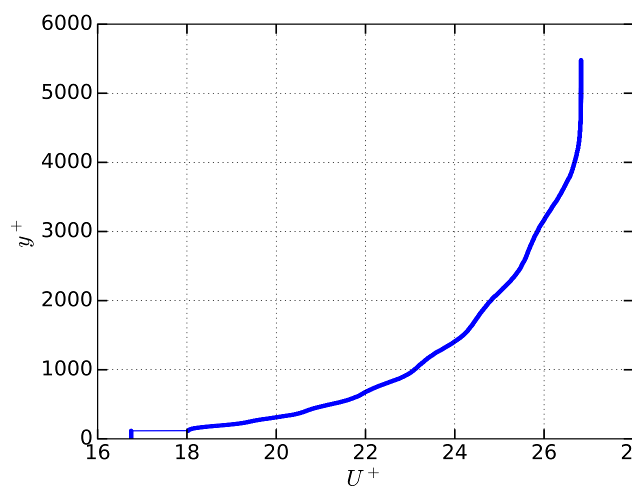

FIG. 4. Mean stream-wise velocity profile for 5000 independent realizations with a Gaussian perturbation of $\mu = 0$ and $\sigma = 0.4$.

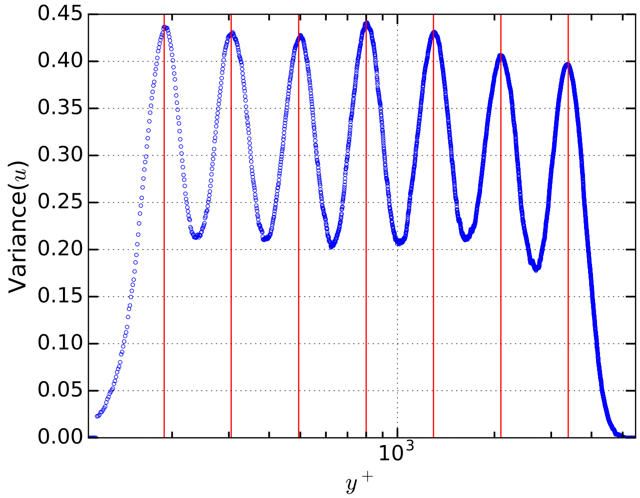

FIG. 5. Stream-wise velocity variance for 5000 independent realizations with a Gaussian perturbation of $\mu = 0$ and $\sigma = 0.4$. Red vertical solid lines denote the original position of the vortical fissures.

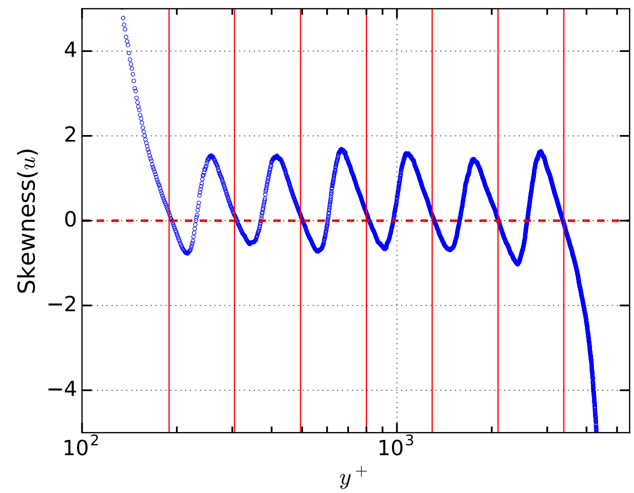

FIG. 6. Skewness of streamwise velocity fluctuations for 5000 independent realizations with a Gaussian perturbation of $\mu = 0$ and $\sigma = 0.4$ (open circles). The skewness for a Gaussian distribution is plotted as reference (red dashed horizontal line) and the red vertical solid lines denote the original position of the vortical fissures.

region (Layer III table), i.e. it is maximum in the proximity of the wall and then it reaches its maximum negative value close to the boundary layer thickness $y^+ = \delta^+$. However through the inertial region the skewness oscillates with an small amplitude of ± 1 units around the value for a Gaussian distribution, in contrast with the experimental data that shows a plateau tendency right below of the Gaussian trend. The oscillations in the skewness are also a side-effect of the probability perturbation in the position of the vortical fissures. Unlike the skewness, the oscillations for the stream-wise velocity kurtosis (Fig. 7) have a higher amplitude trough the inertial region where the experimental data exhibit an uniform subgaussian trend. This behaviour does not reproduce properly the turbulence statistics and thus we explore higher values of σ in the Gaussian perturbation.

In the second scenario $\sigma = 1$ is selected in order to achieve a more homogeneous velocity distribution. This perturbation creates a random vertical motion of the vortical fissures between -300% and 300% of their respective step height (see Sec. II B). Consequently the vortical fissures in the upper edge of the inertial region can cross and reside close to the wall. The opposite is also true for vortical motions that lie in the onset of the inertial region. Fig. 8 shows a smoother profile compared with $\sigma = 0.4$ where peak-locking effect was still present. This mean velocity profile exhibits a good agreement for $\delta^+ = 5200$ respect to the experimental data. In addition to the mean, the second, third and fourth order moments are also computed for this scenario. Fig. 9 reveals some of the main properties of the stream-wise velocity variance for turbulent flows. These are, the variance is zero in the vicinity of the wall with its maximum value in the onset of the logarithmic region and then decreases almost logarithmically toward the boundary layer edge $y^+ = \delta^+$.

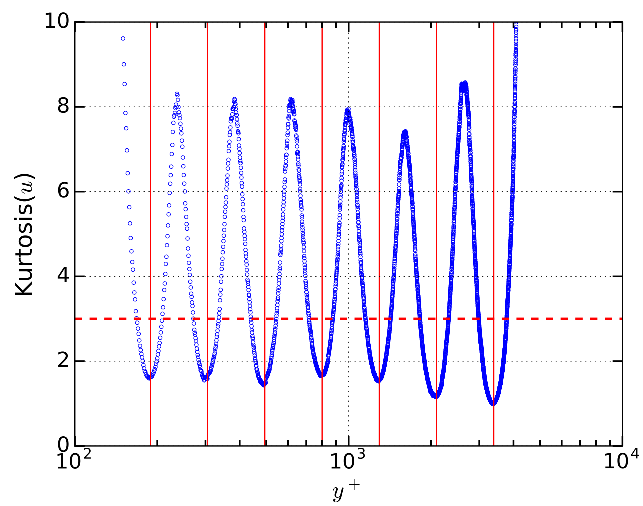

FIG. 7. Kurtosis of streamwise velocity fluctuations for 5000 independent realizations with a Gaussian perturbation of $\mu = 0$ and $\sigma = 0.4$ (open circles). The kurtosis for a Gaussian distribution is plotted as reference (red dashed horizontal line) and the red vertical solid lines denote the original position of the vortical fissures.

Although the variance is not totally smooth, it is a good improvement over the variance for the first scenario. Also note there is not evidence of peak-locking effect like can be visualized in the third and fourth moments (Figs. 10 and 11). Fig. 10 shows the skewness for $\sigma = 1$, it can be appreciated how the skewness has its maximum positive value close to the wall and then when it is approaching to the log region exhibits a subgaussian trend that rapidly decays to its maximum negative peak at the end of the

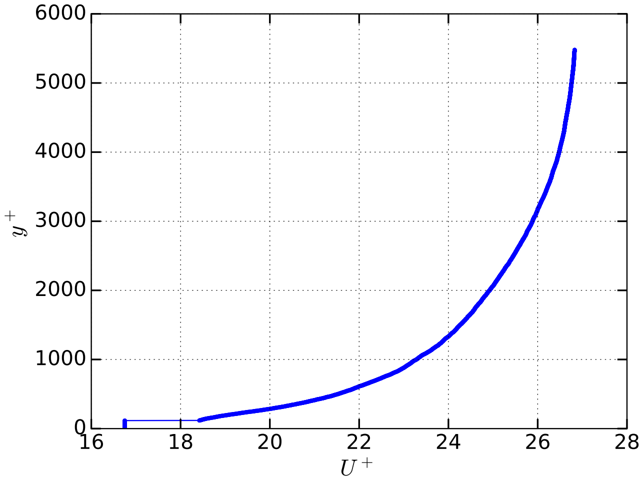

FIG. 8. Mean turbulent stream-wise velocity profile for 5000 independent realizations with a Gaussian perturbation of $\mu = 0$ and $\sigma = 1$.

logarithmic region. Unlike the experimental results, the boundaries of the skewness in the toy model still do not show the adequate trend. This is caused mainly because the first and last step vortical positions in the model are not being perturbed. Further investigation is necessary to establish the proper boundary conditions near to the wall and away from it, in order to improve the streamwise velocity statistics. Observation of Fig. 11 evidences a similar pattern for the streamwise kurtosis, where the behaviour of the trend in the boundaries does not reproduce the experimental results faithfully. Despite of these discrepancies, the kurtosis is very well behaved in the inertial region where it exhibits a subgaussian trend similar to the real data. Experimentally, it is expected that the kurtosis reach its maximum value at $y^+ \approx \delta^+$ and then

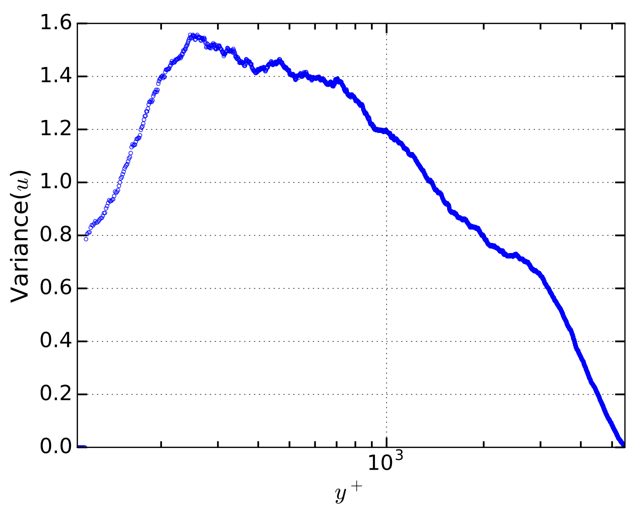

FIG. 9. Stream-wise velocity variance for 5000 independent realizations with a Gaussian perturbation of $\mu = 0$ and $\sigma = 1$.

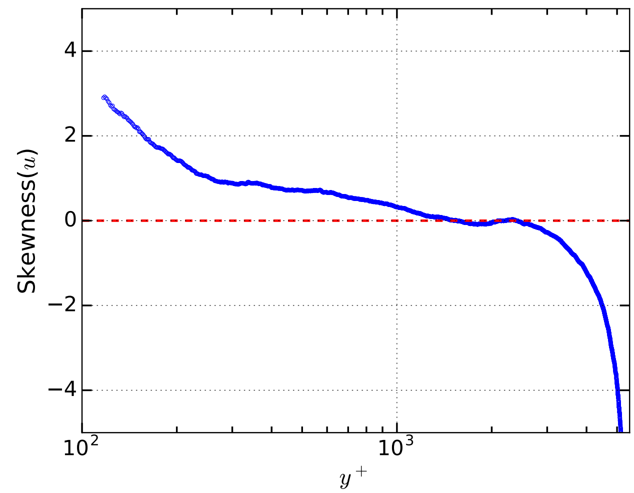

FIG. 10. Skewness of streamwise velocity fluctuations for 5000 independent realizations with a Gaussian perturbation of $\mu = 0$ and $\sigma = 1$ (open circles). The skewness for a Gaussian distribution is plotted in red dashed lines as reference.

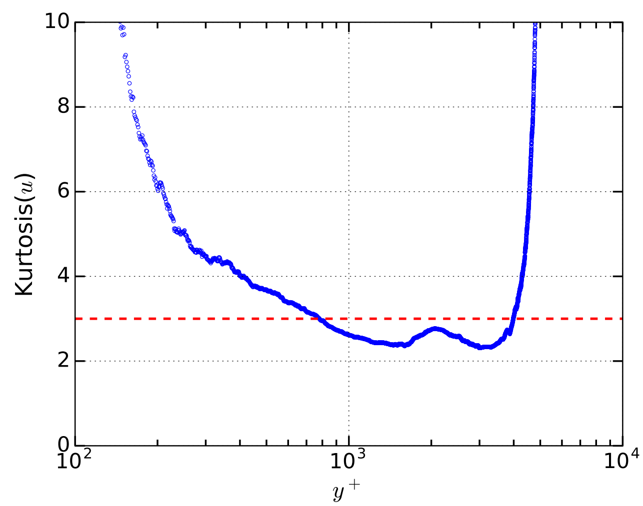

FIG. 11. Kurtosis of streamwise velocity fluctuations for 5000 independent realizations with a Gaussian perturbation of $\mu = 0$ and $\sigma = 1$ (open circles). The kurtosis for a Gaussian distribution is plotted in red dashed lines as a reference.

decay in the free-stream region outside to the boundary layer [20]. This is not observed in our results due to the boundary conditions explained previously. However a new distribution to perturb the position of the vortical fissures is attempted, one whose edges decays smoother than the gaussian distribution, thus a dependence on the perturbation distribution can be discarded. Next section describe the numerical results of the turbulence statistics using an uniform distribution.

B. Uniform distribution

Previous section suggest that the vortical fissure crossing enhances the creation of a more homogeneous velocity distribution in the boundary layer, therefore different percentages of perturbation for the uniform distribution were explored. It was found that percentages $\leq 130\%$ results in big oscillations as described in Sec III A for $\sigma = 1$. We also noted that for perturbations $\geq 200\%$, the shape of the streamwise statistics is in strong disagreement with the real data. As a consequence, an uniform distribution between -150% and 150% of the height of the step was selected. Fig. 12 shows the streamwise velocity profile for the uniform perturbation. In comparison with Fig. 4, the jumps in the velocity profile seem to increase more linearly (see inset in Fig. 4). This is a consequence of the uniform distribution perturbation, where each vortical positions have the same probability to occur.

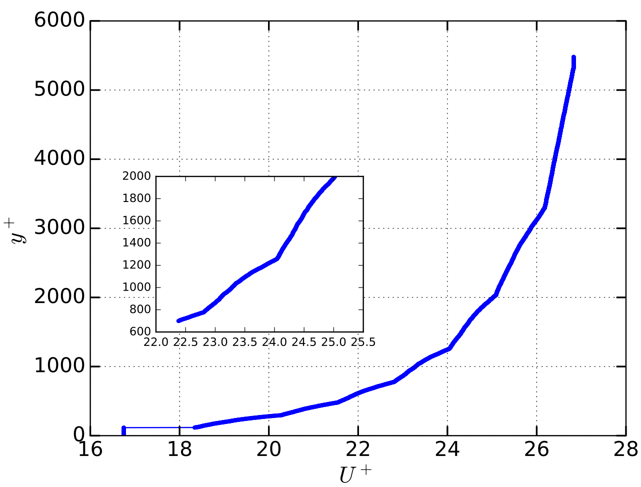

FIG. 12. Mean turbulent stream-wise velocity profile for 5000 independent realizations with an uniform perturbation of $\pm 150\%$. In the inset, the velocity peaked area from $y^+ = 700$ to $y^+ = 2000$.

This effect can be appreciated more clearly in the stream-wise velocity variance (Fig. 13), where the variance has maximum locals around the geometric center of the unperturbed vortical positions (red solid vertical lines). These oscillations have a similar amplitude (~ 0.2 units) to the Gaussian perturbation for $\sigma = 0.4$ (Fig. 5). Despite of the oscillations, the main features of the turbulence variance are conserved. For instance, the maximum value for the variance is in the proximity of the wall, and then a pronounced negative slope is extended in the inertial region up to reach zero in the edge of the boundary layer.

The rapid variations still persist in the higher order moments, however their amplitude are smaller compared with the gaussian distribution for $\sigma = 0.4$. Fig. 14 shows the skewness of the streamwise velocity for an uniform distribution. A strong agreement in the main features

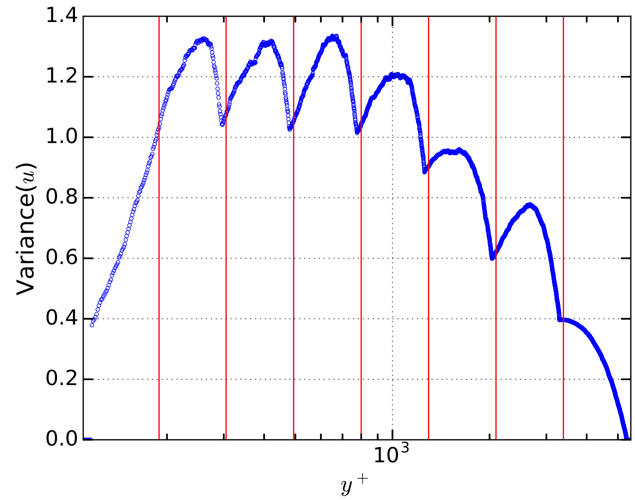

FIG. 13. Variance of streamwise velocity fluctuations for 5000 independent realizations with an uniform perturbation of $\pm$%150. Red vertical solid lines denote the original position of the vortical fissures

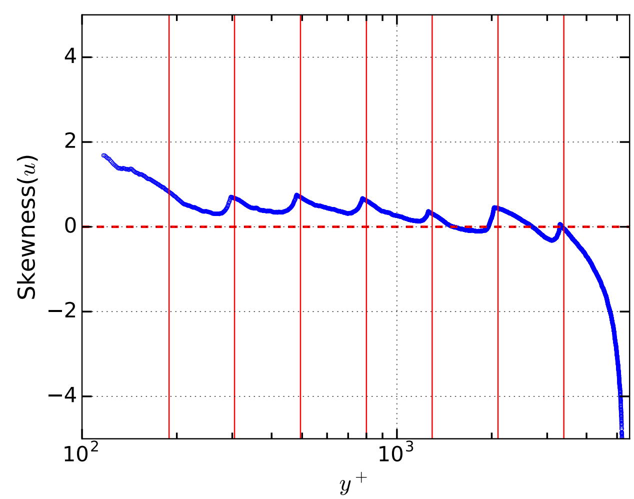

FIG. 14. Skewness of streamwise velocity fluctuations for 5000 independent realizations with an uniform perturbation of $\pm 150\%$ (open circles). The skewness for a Gaussian distribution is plotted as reference (red dashed horizontal line) and the red vertical solid lines denote the original position of the vortical fissures.

between the numerical simulation and the experimental skewness is observed, in brief the skewness follows a pseudo-Gaussian trend in the inertial region , then it increases up to reach its maximum negative value in the upper limit of the boundary layer $y^+ = \delta^+$ to after finally decaying to zero in the free-stream region. Fourth order moment is illustrated in Fig. 15, the trend is in complete concordance with the experimental data if the small oscillations are neglected. Further exploration is needed to improve the right behaviour in the upper and lower limits of the inertial region.

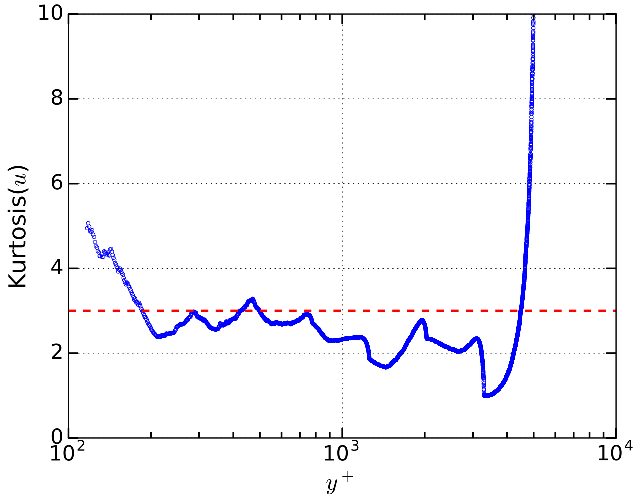

FIG. 15. Kurtosis of streamwise velocity fluctuations for 5000 independent realizations with an uniform perturbation of ±130% (open circles). The kurtosis for a Gaussian distribution is plotted in red dashed lines as a reference.

IV. CONCLUSIONS

Several statistical distributions were used to reproduce the structure of the streamwise velocity statistics. It was found that the Gaussian and the uniform distribution exhibit a good agreement with the experimental data. The results also reveal that in order to reproduce adequately the streamwise velocity statistics, it is necessary that the vortical fissures cross through the boundary layer. Hence that the percentages of perturbation for the Gaussian and uniform perturbation that satisfy this condition are 100% and 150% respectively. Higher percentages were also explored but there were not either qualitative or quantitative improvements in the statistics. Further observation of the mean streamwise-velocity profile allows to infer that an inertial region in the turbulent boundary layer exist between $y^+ = 10^3$ through $y^+ = 3 \times 10^3$ approximately. Careful observations of the third and fourth order moments indicate that an inertial region in the turbulent boundary layer exist between $y^+ \approx 2 \times 10^2$ through $y^+ = 4 \times 10^3$ (Layer II to Layer IV in table I). These results support the main hypothesis of this paper, namely the boundary layer structure is the result of the long-time averaged of instantaneous velocity profiles with different distributions of UMZs. For the present model, Eqs. A2 and A3 describe reasonably the mean and the streamwise velocity variance for any statistical perturbation, however further calculations are necessary to develop a theoretical expression for the third and fourth order moments.

ACKNOWLEDGMENTS

The author would like to thank Dr Christhopher M. White and Joseph Klewicki by their valuable discussions and contributions to this paper and the PhD student Alireza Ebadi for elaborating the mathematical model and writing the appendix A.

Appendix A: Distribution of vortical fissures

Consider M vortical fissures in the boundary layer, each with a characteristic velocity of u_k, where $k = [1 : M]$. Based on the definition of the uniform momentum zones, velocity at each wall-normal position, u_k is the characteristic velocity of the closest upper fissure. Now, the wall-normal position of each fissure is perturbed N times with a normalized probability density function P_k. For each wall-normal position, there will be a velocity time series $u(y,t)$. The velocity time series is a selection of characteristic velocities of the vortical fissures, i.e., $u(y,t) = [N_1 u_1, N_2 u_2, ..., N_M u_M]$, where $t = [1 : N]$ and N is the number of realizations. In order to calculate the statistical moments at each wall-normal position (y_0), one needs to find the coefficients $N_k(y_0)$, which is the number of times that the characteristic velocity u_k is experienced at that location, e.g.,

$N_k(y_0)$ = (Probability of having vortical fissure k as the closest upper fissure) $\times$ N.

Therefore the probability of having vortical fissure k as the closest upper fissure = (Probability of having vortical fissure k above y_0) $\times$ (Probability of not having any other vortical fissure between y_0 and location of fissure k) or in mathematical notation

$$N_k(y_0) = N \int_{y_0}^{\delta} P_k(y) \prod_{j=1}^{M(j \neq k)} \left(1 - \int_{y_0}^{y} P_j(\eta) d\eta\right) dy. \tag{A1}$$

Using Eq. A1, one can calculate the statistical moments as follow:
Mean:

$$\overline{u}(y_o) = \frac{1}{N} \sum_{k=1}^{M} N_k(y_0) u_k \tag{A2}$$

Variance:

$$\overline{u'^2}(y_o) = \frac{1}{N} \sum_{k=1}^{M} N_k(y_0)(u_k - \overline{u}(y_0))^2 \tag{A3}$$

[1] S. J. Kline, W. C. Reynolds, F. A. Schraub, and P. W. Runstadler, Journal of Fluid Mechanics **30**, 741 (1967).
[2] M. R. Head and P. Bandyopadhyay, Journal of Fluid Mechanics **107**, 297 (1981).
[3] D. K. Heist, T. J. Hanratty, and Y. Na, Physics of Fluids **12**, 2965 (2000).
[4] C. D. Meinhart and R. J. Adrian, Physics of Fluids **7**, 694 (1995).
[5] R. J. Adrian, C. D. Meinhart, and C. D. Tomkins, Journal of Fluid Mechanics **422**, 1 (2000).
[6] P. Priyadarshana, J. Klewicki, S. Treat, and J. Foss, Journal of Fluid Mechanics **570**, 307 (2007).
[7] S. C. Morris, S. R. Stolpa, P. E. Slaboch, and J. C. Klewicki, Journal of Fluid Mechanics **580**, 319 (2007).
[8] C. M. de Silva, N. Hutchins, and I. Marusic, Journal of Fluid Mechanics **786**, 309 (2016).
[9] H. Tennekes, Physics of Fluids (1958-1988) **11**, 669 (1968).
[10] R. J. Adrian, Physics of Fluids **19**, 041301 (2007), 10.1063/1.2717527.
[11] A. E. Perry and I. Marusic, Journal of Fluid Mechanics **298**, 361 (1995).
[12] M. Lee and R. D. Moser, Journal of Fluid Mechanics **774**, 395 (2015).
[13] H. Tennekes and J. Lumley, *A First Course in Turbulence* (MIT, Cambridge, 1972).
[14] P. A. Davidson, *Turbulence: an introduction for scientists and engineers* (Oxford University Press, USA, New York, 2004).
[15] J. Mathieu and J. Scott, *An Introduction to Turbulent Flow* (Cambridge, Cambridge, 2000).
[16] T. Wei, P. Fife, J. Klewicki, and P. McMurtry, Journal of Fluid Mechanics **522**, 303 (2005).
[17] P. Fife, T. Wei, J. Klewicki, and P. McMurtry, Journal of Fluid Mechanics **532**, 165 (2005).
[18] J. Klewicki, P. Fife, T. Wei, and P. McMurtry, Philosophical Transactions of the Royal Society of London A: Mathematical, Physical and Engineering Sciences **365**, 823 (2007).
[19] J. Klewicki, J. Philip, I. Marusic, K. Chauhan, and C. Morrill-Winter, Phys. Rev. E **90**, 063015 (2014).
[20] P. Vincenti, J. Klewicki, C. Morrill-Winter, C. M. White, and M. Wosnik, Experiments in Fluids **54**, 1 (2013).
[21] J. F. Morrison, B. J. McKeon, W. Jiang, and A. J. Smits, Journal of Fluid Mechanics **508**, 99 (2004).